Journal of
Synchrotron
Radiation

ISSN 0909-0495

Received 26 May 2006
Accepted 27 November 2006

Tracking X-ray-derived redox changes in crystals of a methylamine dehydrogenase/amicyanin complex using single-crystal UV/Vis microspectrophotometry

Arwen R. Pearson,[a] Reinhard Pahl,[b] Elena G. Kovaleva,[a] Victor L. Davidson[c] and Carrie M. Wilmot[a]*

[a]Department of Biochemistry, Molecular Biology and Biophysics, The University of Minnesota, Minneapolis, MN 55455, USA, [b]Consortium for Advanced Radiation Sources, University of Chicago, Chicago, IL 60637, USA, and [c]Department of Biochemistry, The University of Mississippi Medical Center, Jackson, MS 39216, USA. E-mail: wilmo004@umn.edu

X-ray exposure during crystallographic data collection can result in unintended redox changes in proteins containing functionally important redox centers. In order to directly monitor X-ray-derived redox changes in trapped oxidative half-reaction intermediates of *Paracoccus denitrificans* methylamine dehydrogenase, a commercially available single-crystal UV/Vis microspectrophotometer was installed on-line at the BioCARS beamline 14-BM-C at the Advanced Photon Source, Argonne, USA. Monitoring the redox state of the intermediates during X-ray exposure permitted the creation of a general multi-crystal data collection strategy to generate true structures of each redox intermediate.

Keywords: single-crystal microspectrophotometry; reaction intermediates; structural enzymology; tryptophan tryptophylquinone; methylamine dehydrogenase.

1. Introduction

Structural enzymology uses X-ray crystallographic techniques to determine structures of intermediates and intermediate analogues in order to probe mechanisms proposed from other techniques such as UV/Vis spectroscopy (Bourgeois & Royant, 2005). Many enzymes retain their catalytic activity in the crystalline state, and soaking-in or co-crystallization with a substrate can result in the structure of an intermediate or product complex. Many recent studies have taken advantage of UV, visible or Raman spectroscopic signals from reaction intermediates generated during turnover to track the progress of catalysis in crystals using specially designed single-crystal microspectrophotometers (Pearson *et al.*, 2004). These are of two kinds: on-line spectrophotometers which are mounted onto or around the goniostat and permit spectra to be recorded during X-ray exposure, or off-line spectrophotometers which require the crystal to be transferred between instruments to record spectroscopic and X-ray diffraction data. The availability and configuration of these instruments has been recently reviewed (Pearson *et al.*, 2004). Most of these instruments are custom built; however, a modular system is now commercially available that can be used off-line, and with some customization also on-line (Hadfield & Hajdu, 1993).

Intermediates along the reaction pathway can be trapped either kinetically or mechanistically (Bourgeois & Royant, 2005). In kinetic trapping, advantage is taken of the fact that catalysis often proceeds much more slowly in the crystal than in solution. This is attributed to a combination of solvent and crystal packing effects (Wilmot *et al.*, 2002). The slowing down of catalysis in the crystal can result in the accumulation of individual intermediates that can be freeze trapped for structural analysis. Mechanistic trapping, on the other hand, stops the reaction at precise points by altering the conditions under which the reaction is being carried out. For example, if a reaction step requires deprotonation, placing the crystal in low pH buffer can slow or prevent this step in order to accumulate the protonated intermediate (Merli *et al.*, 1996).

We used mechanistic trapping techniques and single-crystal visible microspectrophotometry (SCVM) to track and trap the oxidative half-reaction intermediates of the bacterial enzyme methylamine dehydrogenase (MADH) from *Paracoccus denitrificans* (Pearson & Wilmot, 2003). MADH contains a novel protein-derived cofactor tryptophan tryptophylquinone (TTQ) that is synthesized from two endogenous tryptophan residues (Fig. 1*a*) (McIntire *et al.*, 1991).

MADH catalyses the conversion of methylamine to formaldehyde in a reductive half-reaction, leaving the TTQ in a $2e^-$ reduced state (TTQ_{NQ}; Fig. 1*b*) (Davidson, 2005). TTQ_{NQ} is reoxidized by two sequential electron transfers (ET) to a specific ET partner, the blue copper protein amicyanin (Husain & Davidson, 1985), yielding first the TTQ N-semiquinone radical (TTQ_{NSQ}) and then the fully oxidized N-

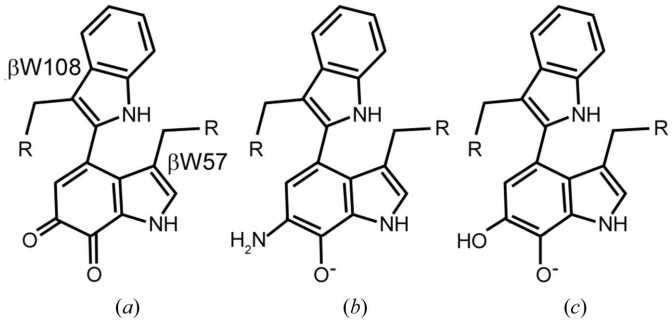

Figure 1
(*a*) Tryptophan tryptophylquinone (TTQ) derived from residues βW57 and βW108 of *P. denitrificans* MADH. (*b*) N-quinol form of TTQ after substrate reduction. (*c*) O-quinol form of TTQ after reduction by dithionite.

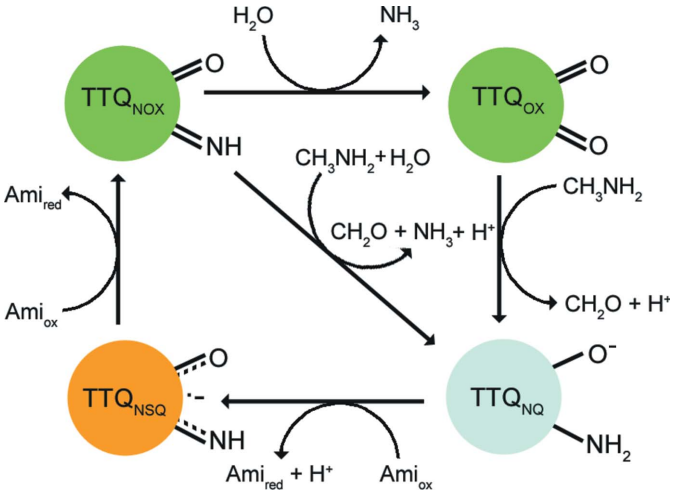

Figure 2
Schematic representation of the MADH catalytic cycle.

quinone, which rapidly releases ammonia, either through hydrolysis to the resting state of the enzyme (TTQ_{OX}) or through direct attack by a second molecule of methylamine to re-enter the catalytic cycle (Fig. 2).

MADH can also be reduced chemically by reductants such as sodium dithionite. In this case there is no displacement of a TTQ oxygen by the amine group of substrates, and the reduction results in an O-quinol (TTQ_{OQ}; Fig. 1*c*). Oxidation of TTQ_{OQ} then proceeds *via* an O-semiquinone radical (TTQ_{OSQ}) (Husain *et al.*, 1987).

Amicyanin is in turn oxidized by a cytochrome which transfers the electrons into the terminal oxidation pathway, providing energy for the cell (Husain & Davidson, 1986). MADH can be crystallized in a binary complex with amicyanin which is competent both for catalysis and ET (Chen *et al.*, 1992). Both TTQ and the copper center of amicyanin have distinct visible spectral signatures (Table 1) which allow precise identification of the redox species present in the crystal (Merli *et al.*, 1996; Pearson & Wilmot, 2003).

During initial synchrotron X-ray data collection, we noted that the crystals containing oxidized species were changing color, indicative of a change in redox state that was later confirmed by off-line SCVM following data collection. In order to investigate the X-ray radiation driven changes more accurately, we mounted the optical system of the 4DX Systems microspectrophotometer on-line at BioCARS beamline 14-BM-C at the Advanced Photon Source (APS). The multiplicity of possible redox species that could exist concurrently within the crystals of the MADH/amicyanin electron transfer complex made the determination of a data collection strategy, which would allow us to collect complete data sets for each intermediate, particularly challenging. Here we demonstrate that crystals undergoing 'dummy' X-ray data collection conditions, where they are not rotated during X-irradiation, can be used to define a maximum X-ray dose allowed for each experimental crystal. This knowledge can be used to assemble composite data sets, in which data from multiple crystals are merged, or where a single crystal is translated discontinuously during data collection.

Table 1
λ_{max} and associated extinction coefficients for MADH and amicyanin redox states (Husain *et al.*, 1987; Husain & Davidson, 1986).

	Extinction coefficient (M^{-1} cm^{-1})			
Redox state	330 nm	428 nm	440 nm	595 nm
TTQ_{OX}	20600	25200	26200	7400
$TTQ_{N/OQ}$	56400	1800	1200	700
$TTQ_{N/OSQ}$	25200	50400	32400	5700
Cu^{2+}	300	200	300	4600
Cu^{+}	300	100	100	0

2. Experimental

The crystallization of the MADH/amicyanin binary complex was carried out as previously described (Chen *et al.*, 1992). The mechanistic trapping of the MADH N-semiquinone and N-quinol intermediates in the MADH/amicyanin binary complex crystals has also been described elsewhere (Merli *et al.*, 1996; Pearson & Wilmot, 2003).

2.1. Installation of the on-line single-crystal visible microspectrophotometer

The modular system obtained from 4DX Systems AB, Sweden, comprises a base mount, two focusing optics, a goniometer and viewing microscope (Hadfield & Hajdu, 1993). A xenon lamp (Zeiss, Germany) provides the illumination for spectral studies, and the spectra are collected and recorded using an imaging spectrograph (Thermo-Oriel, CT, USA) and DB401-UV CCD detector (Andor Technology, UK). Quartz fiber-optic light guides are used to transfer the light between the lamp, optics and spectrophotometer.

To convert the 4DX system to an on-line microspectrophotometer, the focusing optics were mounted perpendicular to the X-ray beam and the goniometer axis. The customized assembly at BioCARS beamline 14-BM-C allowed combined and individual motion of the optical elements such that the illumination and detection arm of the spectrophotometer could be aligned to the center of rotation of the κ-diffractometer and therefore onto the sample (Fig. 3). In

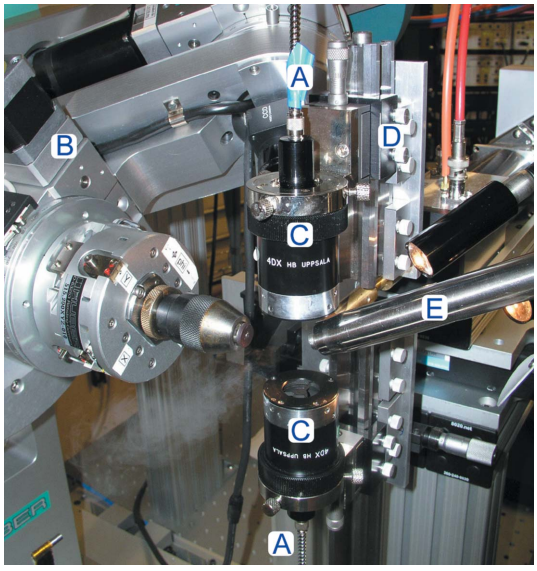

Figure 3
The 4DX Systems microspectrophotometer optics mounted on-line at BioCARS beamline 14-BM-C. A: fiber-optic light guides. B: κ-diffractometer. C: 4DX focusing optics. D: custom mount for 4DX optics. E: cryostream.

detail, the alignment of the 4DX optics was accomplished with the use of a pinhead mounted at the center of the goniometer and adjusting each optic so that light emitted from it was focused precisely at the tip of the pinhead. The focused spot size (measurement area) of light on the crystal is $\sim$0.1 mm (Hadfield & Hajdu, 1993). This alignment procedure ensures that the visible light and the X-ray beam coincide at the sample position. Constraints were programmed into the beamline control software to prevent collision of the goniometer with the light optics during data collection ($\omega = 35^\circ$, $\kappa =$ 0–30°, $\varphi =$ 0–360°, beamstop $d_{\rm min} = 25$ mm). The φ-axis was used as the rotation axis during data collection. The fiber optic light guides allowed the xenon lamp, spectrograph, CCD detector and control computer to be located at a convenient site within the experimental station. Use of a VPN software package allowed remote access to the spectrograph computer and therefore near simultaneous initiation of X-ray and visible spectra data collection.

2.2. Data collection

2.2.1. Single-crystal visible-light microspectrophotometry. Oxidative half-reaction intermediates in MADH/amicyanin crystals were prepared as previously described, and frozen in cryo-loops for data collection (Pearson & Wilmot, 2003). Visible spectra of all crystals were recorded before X-ray exposure to confirm that the desired intermediate was present in the crystal. Spectra were recorded during X-ray exposure of the crystals, both during normal oscillation diffraction data collection and on stationary, *i.e.* non-oscillating, crystals for which diffraction data were not recorded. Recorded spectra at each time point were the average of thirty 19 ms exposures. Data collection was controlled, and analysis of these spectra was carried out, using the Andor *MCD* software package (Andor Technology, UK) supplied with the CCD detector.

Single-wavelength time courses most indicative of changes in each redox species were extracted from the recorded spectra, and rate constants derived by fitting the observed data to a function with a single or double exponential followed by a linear term using the *Biokine* software package (v3.26, Kromatek, UK). Kinetic simulation and fitting of the single-wavelength time courses to determine microscopic rate constants were carried out *via* a stepwise approach using *Dynafit* (Kuzmic, 1996).

2.2.2. X-ray data collection. Complete experimental diffraction data sets were collected from multiple crystals of each reaction intermediate with the ADSC Quantum 315 detector at beamline 14-BM-C. The X-ray wavelength was set to 0.9 Å, and crystals frozen at 104 K were oscillated 0.5° for each image acquisition, and data collection was controlled using beamline-specific software. The beam size was adjusted to $\sigma^2 \simeq 0.1$ mm $\times$ 0.1 mm to match the focused light profile of the microspectrophotometer optics, and so that these were smaller than the crystals (0.7 mm $\times$ 0.3 mm $\times$ 0.3 mm, bipyramidal). For each crystal, one initial diffraction image was collected and indexed, then *PREDICT* (Noble, 1996) was used to identify the optimal orientation to continue data collection in order to obtain as complete a data set as possible for a small angular oscillation range from multiple crystals.

For the data sets used to calculate X-irradiation-induced reduction rates at each redox center, similar sized crystals were subjected to identical data collection conditions as the experimental crystals, except that the crystals were not rotated, thus maintaining their orientation to the microspectrophotometer optics.

The X-ray dose received by each of the crystals was calculated using *RADDOSE* (Murray *et al.*, 2004).

3. Results

During initial X-ray data collection on MADH trapped oxidative half-reaction intermediates at SBC-CAT (beamline 19-BM at APS), we observed that all crystals were bleached along the path of the incident beam following data collection, regardless of their starting oxidation state. Using an off-line 4DX Systems SCVM set-up we confirmed that reduction to TTQ_{NQ}/Cu^{+} or TTQ_{OQ}/Cu^{+} had occurred in all crystals.

During subsequent X-ray data collection at BioCARS beamline 14-BM-C, we also observed X-ray reduction of all crystals tested (TTQ_{OX}/Cu^{2+}, TTQ_{NSQ}/Cu^{+} and TTQ_{NQ}/Cu^{2+}). In order to more accurately monitor the rate of reduction in the X-ray beam at the two redox centers, and remove any errors arising from crystals not being oriented identically when transferred back and forth between the X-ray diffraction camera and the off-line microspectrophotometer, we mounted the 4DX system on-line at BioCARS beamline 14-BM-C.

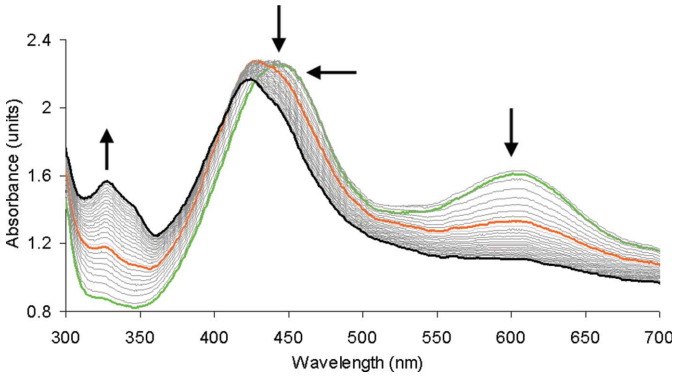

Figure 4
Reduction of oxidized O-quinone MADH/amicyanin crystals (TTQ_{OX}/Cu^{2+}) by X-ray illumination. Spectra were recorded at 1 s intervals, but for clarity only the first 5 min of exposure (X-ray dose $\simeq 9.3 \times 10^5$ Gy) and spectra recorded every 10 s are shown. Arrows indicate the direction of change for the main features; note that there is a transient increase at ~428 nm as the TTQ_{OSQ} forms and then decays. The starting and ending spectra are shown in green and black, respectively; the orange spectrum shows maximum TTQ_{OSQ} content.

3.1. Single-crystal visible-light microspectrophotometry

We first attempted to record single-crystal visible spectra during X-ray data collection. However, the resulting series of spectra were very difficult to interpret. Single-crystal spectra are anisotropic, which can lead to large changes when the crystal orientation is altered, and this is a particular problem in the case of planar chromophores like TTQ. However, with careful alignment a 'sweet spot' can often be found where the anisotropic spectrum qualitatively resembles the isotropic solution spectrum. This corresponds to the direction where there is the greatest mix of chromophore orientations projected through the crystal. When MADH/amicyanin crystals were rotated during data collection, there were marked orientation effects which made it difficult to determine whether the changes were due to X-ray exposure or to anisotropy (see supplementary data[1]). We decided to explore whether we could use crystals equivalent to those used for the experimental diffraction data collection, but record from these only the changes in their absorbance spectra during an identical pseudo-data collection, *i.e.* where the crystal is not rotated out of the 'sweet spot'.

In order to obtain a valid comparison between the crystals used to monitor spectral changes and those used for structure determination, multiple crystals of each intermediate were monitored for spectral changes during equivalent X-ray exposure (X-ray flux $\simeq 2 \times 10^{11}$ photons s^{-1}). The recorded spectra indicated that reduction of the TTQ and copper sites in the MADH/amicyanin crystals occurred rapidly, with 20% reduction occurring in less than 1 min for both redox sites (Fig. 4).

There was a trade-off between the exposure time and resolution as an exposure of 1.5–2 s was required to collect data with sufficient spatial resolution (<2.25 Å) to be of use in drawing mechanistic conclusions.

Table 2
Observed rate constants derived from the X-ray-induced reduction of an O-quinone/Cu^{2+} crystal.

		Major contributing species	Minor contributing species
k_{428}	0.034 s^{-1}	$TTQ_{N/OSQ}$	TTQ_{OX}
k_{330}	0.005 s^{-1}	$TTQ_{N/OQ}$	TTQ_{OX} and $TTQ_{N/OSQ}$
$k_{600\text{-}1}$	0.007 s^{-1}	Cu^{2+}	TTQ_{OX} and $TTQ_{N/OSQ}$
$k_{600\text{-}2}$	0.022 s^{-1}	Cu^{2+}	TTQ_{OX} and $TTQ_{N/OSQ}$

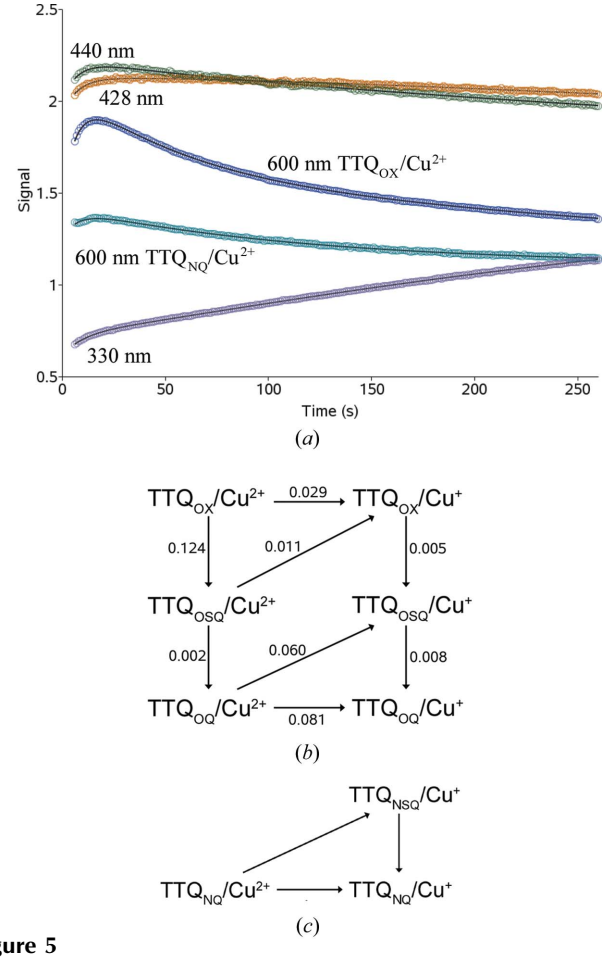

Figure 5
Pathways of X-ray-driven reduction. (*a*) Observed (circles) and simulated (black lines) time courses for reduction of TTQ_{OX}/Cu^{2+}. The simulation curves were calculated using the microscopic rate constants derived from the mechanism in (*b*). Data points are shown for 440 nm, 428 nm, 330 nm, 600 nm (TTQ_{OX}/Cu^{2+} crystal) and 600 nm (TTQ_{NQ}/Cu^{2+} crystal). (*b*) Hypothetical mechanism showing all possible reduction and inter-redox center electron transfers for X-ray reduction of TTQ_{OX}/Cu^{2+}. (*c*) Simpler mechanism for TTQ_{NQ}/Cu^{2+} X-ray-driven reduction.

Catalytic intermediate specific single-wavelength time courses were used to derive observed rate constants for the formation and decay of the various TTQ and copper states during X-ray-driven reduction of an O-quinone (TTQ_{OX}/Cu^{2+}) crystal (Table 2; Fig. 5*a*). These showed that TTQ_{OX} was reduced in two sequential one-electron reductions resulting in the transient formation of TTQ_{OSQ} before further reduction to TTQ_{OQ}. Formation of both TTQ_{OSQ} and TTQ_{OQ} were best fit

[1] Supplementary data for this paper are available from the IUCr electronic archives (Reference: MS5001). Services for accessing these data are described at the back of the journal.

using a single exponential and a linear component; however, the decay of the signal at 600 nm in the O-quinone crystal was best fit using a double exponential followed by a linear component. The amplitudes of each exponential component are very similar. The same analysis was carried out on a second O-quinone crystal and showed that, although the absolute rates determined differed slightly, the overall mechanism was the same, with the TTQ_{OX} reducing first to TTQ_{OSQ} then TTQ_{OQ}, and the 600 nm absorbance indicating two distinct processes.

This suggests that at least two distinct reduction events are occurring at 600 nm. This could reflect different reduction processes at the copper, such as a direct reduction by a photoelectron and reduction by an internal electron transfer from TTQ_{OSQ} or TTQ_{OQ}, or the deposition of two separate photoelectrons. A third possibility is that the two amicyanins in the asymmetric unit differ in their susceptibility to reduction as their surrounding environments are different. However, owing to the not insignificant contributions of other species to each intermediate specific single-wavelength time course (Table 1) and the complications in estimating anisotropic extinction coefficients from the recorded spectra, it is difficult to resolve these possibilities. In an effort to probe the steps in the mechanism that may account for the observed multiphasic reduction processes, we used a stepwise mechanism simulation approach (Fig. 5*a*). In the mechanism shown in Fig. 5(*b*) for reduction of an O-quinone-containing crystal (TTQ_{OX}/Cu^{2+}), both TTQ and copper could be independently reduced, in addition to inter-redox center electron transfer from TTQ to copper. Each step was treated as irreversible owing to the constant influx of photoelectrons. As a consequence, relative or apparent extinction coefficients could be used to relate changes in absorbance to changes in concentration of each species. Involvement of inter-redox center electron transfer appears to be necessary to account for the transient build-up of the absorbance at 600 nm observed when X-ray-driven reduction is initiated within the TTQ_{NQ}/Cu^{2+} crystal. The resulting reduction mechanism for the TTQ_{NQ}/Cu^{2+} crystal is shown in Fig. 5(*c*). The rate constants and apparent extinction coefficients, estimated from the fit of the 600 nm time course for the TTQ_{NQ}/Cu^{2+} crystal data to this simpler mechanism (Fig. 5*c*), were then combined with the 600 nm data for a fully oxidized crystal (TTQ_{OX}/Cu^{2+}) to simulate the full mechanism shown in Fig. 5(*b*). These were consistent with the observed 600 nm time course in the TTQ_{OX}/Cu^{2+} crystals, and the mechanism in Fig. 5(*b*). The overall kinetic parameters were further refined by sequential addition of the time courses at 330, 428 and 440 nm in the simulation (Fig. 5*a*), using well defined estimates from the 600 nm data for both TTQ_{NQ}/Cu^{2+} and TTQ_{OX}/Cu^{2+} crystals to give a set of rate constants that account for observed absorbance changes at all wavelengths (Fig. 5*b*). Although a more extensive detailed kinetic investigation is necessary to confirm the mechanism and the unique set of parameters, the present analysis indicates that the inter-redox center electron transfer represents a plausible pathway consistent with the data.

3.2. X-ray data collection

As a rule of thumb, if a species is present at >80% occupancy in the crystal it will dominate the resulting electron density. We therefore used the reduction of any oxidized species reaching 20% (estimated from the overall decrease in absorbance of each species) as a cut-off criterion to determine the amount of data that could be used from each individual crystal in composite data sets of redox homogeneous intermediates. This conservative approach would give an average 90% occupancy of the oxidized species over the time period of diffraction data collection. We attempted to align all crystals such that the thickest part was in the beam (crystals show a square bipyrimidal morphology). There were variations in the rate of reduction from crystal to crystal, reflecting differences in the thickness and orientation of the crystal at the point of X-ray irradiation, and thus dose delivered within each crystal. For example, in seven O-quinone crystals tested, 20% loss of the 600 nm absorbance occurred at 21, 22, 24, 27, 30, 41 and 48 s. There is over a two-fold difference in these numbers, demonstrating that a significant number of crystals are required to provide a high degree of certainty in the chosen cut-off time using this protocol. We applied the cut-off at 20 s exposure for the TTQ_{OX}/Cu^{2+} (X-ray dose $\simeq 6.2 \times 10^4$ Gy) and TTQ_{NSQ}/Cu^{+} (X-ray dose $\simeq 8.5 \times 10^4$ Gy) intermediates, as the reduction of TTQ appears faster than that of copper. However, for the TTQ_{NQ}/Cu^{2+} intermediate we were able to apply the cut-off at 40 s exposure (X-ray dose $\simeq 1.2 \times 10^5$ Gy; slightly more than 20% reduction of Cu^{2+}). The resulting composite data sets have interesting implications for MADH mechanism and ET, and will be discussed elsewhere (De la Mora *et al.*, 2007).

4. Discussion

Recently, the awareness of X-ray-driven changes in redox centers has increased as a growing number of researchers studying redox active proteins have begun to use single-crystal spectroscopic methods to probe the redox state of their crystals during or after data collection (Matsui *et al.*, 2002; Dubnovitsky *et al.*, 2005; Yano *et al.*, 2005; Karlsson *et al.*, 2000; Schlichting *et al.*, 2000; Sjögren & Hajdu, 2001; Adam *et al.*, 2004; Kort *et al.*, 2004; Berglund *et al.*, 2002; Bamford *et al.*, 2002; Dias *et al.*, 2004; Sato *et al.*, 2004; Unno *et al.*, 2004). X-ray-driven reduction of proteins is believed to occur through the action of water-derived photoelectrons (Garman & Owen, 2006). Redox centers are considerably more sensitive to radiation damage than other parts of a protein and changes can occur much faster than other visible damage, such as disulfide bond breaking and the decarboxylation of glutamates and aspartates (Weik *et al.*, 2000; Ravelli & McSweeney, 2000; Burmeister, 2000; Garman & Owen, 2006; Nave & Garman, 2005).

The generation of composite data sets using multiple crystals, or through translation of a single-crystal following acquisition of a specific X-ray dose, has now been used in several studies to produce redox homogeneous data sets, and

thus determine the structure of X-ray-sensitive species (Dubnovitsky *et al.*, 2005; Adam *et al.*, 2004; Berglund *et al.*; 2002; Cavazza *et al.*, 2006). However, chromophore anisotropy has limited the ability to track accurately redox changes throughout X-ray data collection with static on-line microspectrophotometer optics in most systems (Dubnovitsky *et al.*, 2005; Adam *et al.*, 2004). If the redox changes are not rapid, then spectra can be recorded during X-ray data collection by the crystal being rotated back to the 'sweet spot' orientation at regular intervals (Dubnovitsky *et al.*, 2005). Alternatively, a careful dose assessment of photoreduction can be carried out to guide the experimental data collection strategy (Dubnovitsky *et al.*, 2005; Adam *et al.*, 2004). However, many of the contributions to dose can be difficult to accurately measure, such as beam flux (Murray *et al.*, 2004).

Here we present a more general multi-crystal strategy to produce composite data sets of redox-sensitive intermediates through the use of a specific beamline and a static on-line microspectrophotometer optics mount. We were able to track the reduction of multiple redox species within crystals of the MADH/amicyanin complex undergoing a pseudo-data collection on BioCARS 14-BM-C, with only a two-fold difference in measured allowable X-ray exposure between different crystals. Consistent crystal morphology and size, which was also larger than the X-ray and light beams, were probably important factors in the small range of observed reduction times from crystal to crystal. However, these crystals are far from the ideal case for single-crystal microspectrophotometry, displaying non-ideal morphology for single-crystal microspectrophotometry (bipyramidal) that leads to complicating crystal prism effects and difficulties in estimating crystal volume in the beam. We believe our results indicate a viable strategy to obtain homogeneous oxidized catalytic intermediate structures, where crystal morphology, serious anisotropy and multiple redox centers make an accurate dose and reduction rate assessment difficult.

It is clear that SCVM is a valuable tool in the study of redox-active protein structure. In the future, development of dynamic on-line optics mounts that move with the goniometer, and retain the crystal orientation to the microspectrophotometer during crystal rotation, will enable true simultaneous tracking of redox changes during experimental X-ray data collection. In the meantime, the modifications made to BioCARS beamline 14-BM-C have allowed us to mount the modular 4DX Systems SCVM on-line in order to monitor spectral changes during X-irradiation. The availability of this technique at a US National Facility provides the opportunity for users to take advantage of this methodology, without the need for tedious transfer of crystals between the X-ray beam and an off-line microspectrophotometer.

We would like to thank Teresa De la Mora-Rey and Bryan Johnson for help during data collection, as well as the staff of BioCARS, especially Robert Henning, Spencer Anderson and Vukica Šrajer for support during data collection and useful discussions. We thank Steve Ginell at SBC-CAT for support during the initial studies and data collection on this system. This work was supported by NIH grants GM-66569 (CMW) and GM-41574 (VLD). Use of the Advanced Photon Source was supported by the US Department of Energy, Basic Energy Sciences, Office of Science, under Contract No. W-31-109-Eng-38. Use of the BioCARS Sector 14 was supported by the National Institutes of Health, National Center for Research Resources, under grant number RR07707. Use of the Argonne National Laboratory Structural Biology Center beamline 19-BM at the Advanced Photon Source was supported by the US Department of Energy, Office of Biological and Environmental Research, under Contract No. W-31-109-ENG-38.

References

Adam, V., Royant, A., Nivière, V., Molina-Heredia, F. P. & Bourgeois, D. (2004). *Structure*, **12**, 1729–1740.
Bamford, V. A., Bruno, S., Rasmussen, T., Appia-Ayme, C., Cheesman, M. R., Berks, B. C. & Hemmings, A. M. (2002). *EMBO J.* **21**, 5599–5610.
Berglund, G. I., Carlsson, G. H., Smith, A. T., Szoke, H., Henriksen, A. & Hajdu, J. (2002). *Nature (London)*, **417**, 463–468.
Bourgeois, D. & Royant, A. (2005). *Curr. Opin. Struct. Biol.* **15**, 538–547.
Burmeister, W. P. (2000). *Acta Cryst.* D**56**, 328–341.
Cavazza, A., Contreras-Martel, C., Pieulle, L., Chabrière, E., Hatchikian, E. C. & Fontecilla-Camps, J. C. (2006). *Structure*, **14**, 217–224.
Chen, L. *et al.* (1992). *Biochemistry*, **31**, 4959–4964.
Davidson, V. L. (2005). *Bioorg. Chem.* **33**, 159–170.
De la Mora, T. *et al.* (2007). In preparation.
Dias, J. M., Alves, T., Bonifacio, C., Pereira, A. S., Trincao, J., Bourgeois, D., Moura, I. & Romao, M. J. (2004). *Structure*, **12**, 961–973.
Dubnovitsky, A. P., Ravelli, R. B. G., Popov, A. N. & Papageorgiou, A. C. (2005). *Protein Sci.* **14**, 1498–1507.
Garman, E. F. & Owen, R. L. (2006). *Acta Cryst.* D**62**, 32–47.
Hadfield, A. & Hajdu, J. (1993). *J. Appl. Cryst.* **26**, 839–842.
Husain, M. & Davidson, V. L. (1985). *J. Biol. Chem.* **260**, 14626–14629.
Husain, M. & Davidson, V. L. (1986). *J. Biol. Chem.* **261**, 8577–8580.
Husain, M., Davidson, V. L., Gray, K. A. & Knaff, D. B. (1987). *Biochemistry*, **26**, 4139–4143.
Karlsson, A., Parales, J. V., Parales, R. E., Gibson, D. T., Eklund, H. & Ramaswamy, S. (2000). *J. Inorg. Biochem.* **78**, 83–87.
Kort, R., Komori, H., Adachi, S.-I., Miki, K. & Eker, A. (2004). *Acta Cryst.* D**60**, 1205–1213.
Kuzmic, P. (1996). *Anal. Biochem.* **237**, 260–273.
McIntire, W. S., Wemmer, D. E., Chistoserdov, A. & Lidstrom, M. E. (1991). *Science*, **252**, 817–824.
Matsui, Y., Sakai, K., Murakami, M., Shiro, Y., Adachi, S.-I., Okamura, H. & Kouyama, T. (2002). *J. Mol. Biol.* **324**, 469–481.
Merli, A., Brodersen, D. E., Morini, B., Chen, Z., Durley, R. C., Mathews, F. S., Davidson, V. L. & Rossi, G. L. (1996). *J. Biol. Chem.* **271**, 9177–9180.
Murray, J. W., Garman, E. F. & Ravelli, R. B. G. (2004). *J. Appl. Cryst.* **37**, 513–522.
Nave, C. & Garman, E. F. (2005). *J. Synchrotron Rad.* **12**, 257–260.
Noble, M. E. M. (1996). *PREDICT*, http://biop.ox.ac.uk/www/distrib/predict.html.

Pearson, A. R., Mozzarelli, A. & Rossi, G. L. (2004). *Curr. Opin. Struct. Biol.* **14**, 656–662.
Pearson, A. R. & Wilmot, C. M. (2003). *Biochim. Biophys. Acta*, **1647**, 381–389.
Ravelli, R. B. G. & McSweeney, S. M. (2000). *Structure*, **8**, 315–328.
Sato, M., Shibata, N., Morimoto, Y., Takayama, Y., Ozawa, K., Akutsu, H., Higuchi, Y. & Yasuoka, N. (2004). *J. Synchrotron Rad.* **11**, 113–116.
Schlichting, I., Berendzen, J., Chu, K., Stock, A. M., Maves, S. A., Benson, D. E., Sweet, R. M., Ringe, D., Petsko, G. A. & Sligar, S. G. (2000). *Science*, **287**, 1615–1622.
Sjögren, T. & Hajdu, J. (2001). *J. Biol. Chem.* **276**, 13072–13076.
Unno, M., Matsui, T., Chu, G. C., Couture, M., Yoshida, T., Rousseau, D. L., Olson, J. S. & Ikeda-Saito, M. (2004). *J. Biol. Chem.* **279**, 21055–21061.
Weik, M., Ravelli, R. B. G., Kryger, G., McSweeney, S., Raves, M. L., Harel, M., Gros, P., Silman, I. & Sussman, J. L. (2000). *Proc. Natl. Acad. Sci. USA*, **97**, 623–628.
Wilmot, C. M., Sjögren, T., Carlsson, G. H., Berglund, G. I. & Hajdu, J. (2002). *Methods Enzymol.* **353**, 301–318.
Yano, J., Kern, J., Irrgang, K.-D., Latimer, M., Bergmann, U., Glatzel, P., Pushkar, Y., Biesiadka, J., Loll, B., Sauer, K., Messinger, J., Zouni, A. & Yachandra, V. K. (2005). *Proc. Natl. Acad. Sci. USA*, **102**, 12047–12052.